Development of UHTCMCs via water based ZrB2 powder slurry infiltration and polymer infiltration and pyrolysis

Development of UHTCMCs via water based ZrB_2 powder slurry infiltration and polymer infiltration and pyrolysis

Francesca Servadei, Luca Zoli*, Pietro Galizia, Antonio Vinci, Diletta Sciti
CNR-ISTEC, Institute of Science and Technology for Ceramics, Via Granarolo 64, I-48018 Faenza, Italy

**Author to whom correspondence should be addressed: luca.zoli@istec.cnr.it*

Abstract

C_f/ZrB_2-SiC ultra-high temperature composites were manufactured via aqueous slurry impregnation coupled with polymer infiltration and pyrolysis, using a allylhydrido polycarbosilane precursor. For the first time we used ultra-high modulus pitch-based carbon fibres for the PIP process, investigating three different architectures, 0/0°, 0/90°, and 2D. Microstructure, mechanical properties and oxidation resistance in air at 1650 °C were investigated. As expected, the mechanical properties showed the tendency to decrease with increase of the preforms complexity, due to the higher amount of flaws and residual stresses. For instance, the flexural strength was approaching 500 MPa for 0/0°, 370 MPa for 0/90° and 190 MPa for 2D. The materials showed an optimal resistance to oxidation at 1650 °C thanks to formation of a viscous borosilicate glass that guaranteed a self-healing functionality.

Keywords: self-healing, PIP, oxidation resistance, polycarbosilane, borosilicate glass

1. Introduction

Ultra-High Temperature Ceramics (UHTCs) are borides, carbides and nitrides of early transition metals, possessing melting points exceeding 3000 °C [1], high thermal and electrical conductivity, good ablation resistance and excellent strength retention at elevated temperatures [2–4]. Over the last couple of decades, UHTCs, in particular the transition metal di-borides, have gained a growing interest for use in extreme environments, as in hypersonic aerospace vehicles, atmospheric re-entry vehicles and energy applications [5]. ZrB_2 has been extensively investigated as a potential candidate for the development of reusable Thermal Protection Systems (TPS), because of its relatively low density and high thermal conductivity [6]. However, these materials suffer from catastrophic failure due to their low fracture toughness and poor thermal shock resistance [1]. In addition, the oxidation resistance of ZrB_2 is low at temperatures above 1200 °C because of the evaporation of volatile oxides (B_2O_3) and the formation of a non-protective porous layer of ZrO_2 [7]. Usually, ZrB_2-SiC composites are fabricated to get a better oxidation resistance [8], resulting in the formation of a viscous borosilicate layer in oxidative atmosphere [7].

Carbon fibre-reinforced ceramic matrix composites (CMCs) are promising candidates for components in transportation, defence, nuclear and aerospace fields such as brake systems, gas turbine, facing materials, combustion chambers, thrusters, rocket nozzles, and the noses or leading edges of re-entry vehicles because of their higher strength-to-weight ratio, good toughness and thermal shock resistance at high temperature [9,10]. More demanding applications invoke the introduction of UHTC phases in the matrix to overcome the main limitations of current CMCs in term of maximum temperature of service [11]. Indeed, C/SiC and SiC/SiC display an excellent behaviour below 1600 °C, whilst C/C can be used at temperatures above 3000 °C but it is an ablative material [9].

In the literature, several published works report the fabrication of Ultra-High Temperature Ceramic Matrix Composites (UHTCMCs) by the introduction of UHTC phases into the matrix, using many approaches such as: chemical vapour infiltration (CVI) [12–14], polymer infiltration and pyrolysis (PIP) [15–18], reactive melt infiltration (RMI) [19–21] and slurry infiltration and hot pressing (SI-HP) [22,23]. Several researchers investigated carbon fibre (C_f) reinforced ZrB_2 composites: Wang et al. [24] developed 2D C_f/ZrB_2-SiC composites by slurry infiltration and CVI; by using the same combination of techniques, Li et

al. [25] prepared 2D C_f/SiC-ZrB_2-TaC composites. However, the main drawbacks of CVI are high costs and long processing time [26]. Chen et al. [20] have studied C_f/SiC-ZrC-ZrB_2 composites fabricated via RMI. RMI has the advantage of being quick and cost effective; on the other hand, the composites exhibit poor mechanical properties due to the carbothermal reaction between the fibres and the melt [26]. For UHTCMC manufacturing, slurry infiltration and sintering techniques can be successfully employed [27–29], but fabrication of complex shape components and processing of complex fibre architectures is still challenging.

In comparison, the PIP technique is featured by relatively low processing temperatures, no fibre damage and complex shape capability. The most common way of introducing UHTC phases is by infiltrating carbon fibre preforms with a slurry containing the preceramic polymers and the ceramic powders. For instance, Hu et al. [15] fabricated 2D C_f/SiC-ZrB_2 using a ZrB_2 powder based slurry containing polycarbosilane and divinyl benzene, followed by thermal treatment at 1200 °C, achieving composites with a final UHTC content of 19% and porosity of 23%. Uhlmann et al. [17] prepared 2D C_f/SiC-ZrB_2-TaC composites by adding ZrB_2 and Ta powder within the pre-ceramic slurry of C/SiC, followed by thermal treatment at 1600 °C; these materials exhibited an excellent thermo-chemical resistance despite open porosity was above 20%. Recently, Ran et al. [30] have prepared C_f/C-ZrB_2-SiC through a method of high-solid-loading slurry impregnation and further densified by PIP with a polycarbosilane as SiC precursor, reaching an open porosity of 7% after the eighth pyrolysis carried out at 1400 °C.

Noteworthy, all the aforementioned works have been carried out on PAN-based carbon fibre reinforcement, while a limited number of published works are concerned with the use of uncoated pitch-based carbon fibre as reinforcement in CMCs [28,31,32]. The main reason can be ascribed to lower price, availability on the market and higher versatility in the manufacturing and shaping processes. On the other hand, the use of pitch-based C fibres can be recommended for application in harsh aerospace environment thanks to the superior thermal conductivity, chemical stability and elastic modulus [33]. Moreover, a weak fibre-matrix interface is often obtained thanks to coatings on PAN-based carbon fibres, such as pyrolytic carbon or boron nitride, in order to achieve damage tolerant and high strength composites, whereas pitch-based C fibres have been shown to provide intra-fibre pull-out during fracture even without a coating [34–37].

In our previous investigations water-based slurries were found more effective than polymer-based slurries to infiltrate pitch-based C fibre preforms. [15,28] However in that cases the consolidation of materials was carried out by sintering at 1900°C under 40 Mpa. In this work for the first time, to the best of our knowledge, the design and manufacturing of C_f/ZrB_2-SiC composites were proposed combining uncoated pitch-based carbon fibre cloths as reinforcement, water-based slurry impregnation as way to introduce ZrB_2 and SiC particles into the preform and repeated cycles (six) of polymer (allylhydrido polycarbosilane) infiltration and pyrolysis to pressureless consolidate the material under the mild condition of 1000 °C. The overarching purpose of the work was to compare the microstructural features, mechanical properties and oxidation resistance at 1650 °C of composites with increased fibre preforms complexity, e.g. UD (0/0°, 0/90°) and 2D textures.

2. Experimental

2.1 Materials

Commercial products were used as raw materials for the preparation of ceramic matrix composites: ZrB_2 (Grade B, H.C. Starck, Germany; specific surface area 1.0 m^2/g, particle size range 0.5–6 μm, impurities (wt.%): 0.25 C, 2 O, 0.25 N, 0.1 Fe, 0.2 Hf), α-SiC (Grade UF-25, H.C. Starck, Germany; specific surface area 23–26 m^2/g, D_{50} 0.45 μm, impurities (wt.%): 2.5 O). As preceramic polymer of SiC allyl-hydrido polycarbosilane (StarPCS™ SMP-10, Starfire System Inc., U.S.A; density 0.998 g/cm^3, viscosity 40–100 cPs at 25 °C) was used. A catalyst was used to cross-link the polymer: trimethyl(methylcyclopentadienyl)platinum(IV), $MePtCpMe_3$ (Sigma Aldrich; purity 98%). Unidirectional (UD) and plain woven (2D) pitch based ultra-high modulus carbon fibre fabrics (UF-XN80-300 and PF-XN80-240, Granoc, Japan; fabric areal weight 330 and 240 g/m^2 respectively; yarn: XN80-60S, tensile modulus 780 GPa, tensile strength 3.4 GPa, fibre diameter 10 μm, density 2.17 g/cm^3) were used as carbon fibre fabrics.

2.2 Process

The manufacturing of UHTCMCs consisted in a multistep process that combined impregnation with a water-based slurry containing UHTC particles and consolidation through repetitive cycles of polymer infiltration and pyrolysis (PIP) with SMP-10, see Fig. 1.

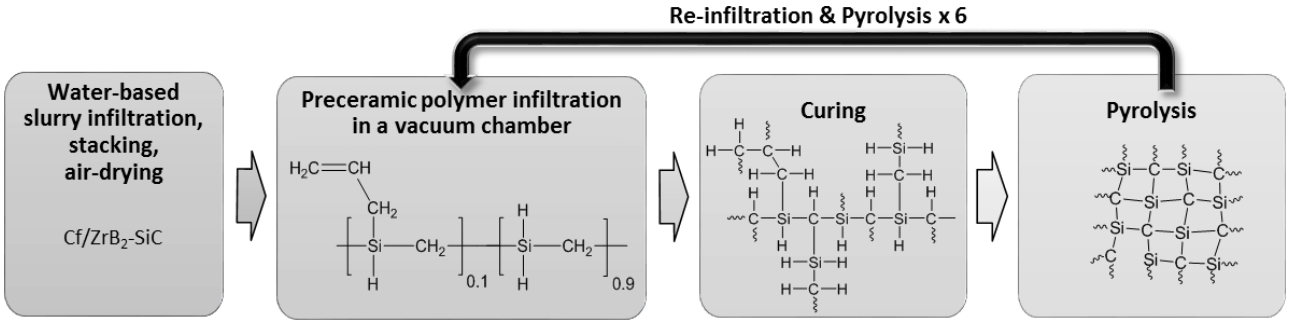

Fig. 1. Multistep process diagram showing UHTCMC manufacturing: 1st step, powder slurry infiltration and stacking of infiltrated fabrics; 2nd step, polymer infiltration of the green composite; 3rd step, crosslinking of polymeric chains (curing); 4th step, conversion of cross-linked resin into ceramic (pyrolsysis).

An aqueous slurry was prepared using a mixture of ZrB_2 – 10 vol.% SiC powders according to previous studies [38]. Four UD or 2D C_f fabrics with approximate dimensions 60 × 100 mm^2 were infiltrated with the aqueous suspension by hand lay-up and subsequently stacked and air-dried at 100 °C for 2 h to produce about 2 mm thick plates (UD fabrics were stacked in 0/0° and 0/90° configurations). Subsequently, impregnated plates were introduced in a glovebox under argon atmosphere for further processing. Inside the glovebox $MePtCpMe_3$ catalyst (0.5 g) was dissolved into 50 g of SMP-10 by stirring the solid catalyst for 15 min; the resulting 1 wt% amber-coloured liquid was used for polymer infiltration. Each plate was placed in a vessel inside a desiccator, located in the glovebox. ~~Air~~Argon was evacuated by a vacuum pump and the composite was subsequently infiltrated by pouring the polymer on the sample until the latter was completely covered. The vacuum was kept for 1 min. After that, the ambient pressure was recovered; infiltrated plates were sealed into plastic bags, taken out from the glove box and transferred into a tubular furnace (HST 12/600 Carbolite, Verder scientific, Italy) under an argon flux of 1 mL/min for curing and pyrolysis. Curing was carried out at 300 °C for 4 h, in order to cross-link the functional groups and convert liquid polymer into a rigid resin. Pyrolysis was carried out at 1000 °C for 2 h. A total of 6 cycles of infiltration with modified SMP-10 (with catalyst) and heat treatment were carried out to achieve the final materials, which were labelled here as 0/0°, 0/90° and 2D.

2.3 Characterization

The final compositions were determined after the pyrolysis cycles. The fibre mass content was calculated considering the fibre areal weight (g/m^2) given by the supplier, number of layers and sample area. The matrix amount added through powder slurry infiltration was then determined as the difference between the infiltrated material weight and fibre weight. After six PIP cycles, 0/0°, 0/90° and 2D samples, bulk densities were measured by the Archimedes' method. Theoretical densities were calculated using the rule of mixtures, relative densities, ρ, were intended as the ratio of bulk and theoretical densities and the residual porosities deduced as 1-ρ. The mercury intrusion porosimetry (MIP) analysis was carried out to determine the amount of open porosities in the range 0.0058-100 μm (Pascal 140 and Pascal 240 series, Thermo Finnigan, U.S.A.). The microstructural features and elemental composition were examined on polished and fractured surfaces by field emission gun-scanning electron microscopy (FE-SEM, Carl Zeiss Sigma NTS Gmbh Öberkochen, Germany) and energy dispersive X-ray spectroscopy (EDS, INCA Energy 300, Oxford instruments, UK). The polished samples for microscopy were prepared by cutting cross sections and polishing them using semi-automatic polishing machine (Tegramin-25, Struers, Italy), then washed with ethanol and acetone in an ultrasonic bath and finally cleaned with a plasma cleaner (Colibrì Plasma RF 50 KHz, Gambetti, Italy) at 40 W for 5 min. Image analysis with a commercial software package (Image-Pro Plus® Analyzer 7.0, Media Cybernetics, U.S.A.) was carried out onto SEM micrographs of polished sections to determine the amounts of C_f, ZrB_2, SiC phases, as well as the mean grain size (m.g.s.) of C_f and ZrB_2. X-ray diffraction patterns were collected from 10°-70° on cross section of 0/0°, 0/90° and 2D samples using a Bruker D8 Advance apparatus with CuKα radiation (Bruker, Karlsruhe, Germany) to analyse the degree of crystallinity of polymer derived silicon carbide after pyrolysis cycles.

Bending tests were carried out on 0/0°, 0/90° and 2D composites at RT, according to ASTM C1341-13 standard for continuous fibre-reinforced advanced ceramic composites. Specimens of 60 mm × 10 mm × as-processed thickness were fractured with a span-to-thickness ratio (s/t) of 20 and a strain rate ($\dot{\varepsilon}$) of 8×10^{-4} s^{-1} by using a universal testing machine (Z050, Zwick Roell, Germany). 3-point bending tests were carried on 0/0° and 0/90° composites with a lower span of 50 mm and 44 mm, respectively. 2D composites were tested through 4-point bending with a lower span of 51 mm and an upper span of 17 mm. 4-point bending test was

chosen instead 3-point bending test because the former allowed to expose at least 8 inter-bundle voids (typical critical flaws of 2D composites [39]) to the maximum stress, and so to avoid invalid tests due to fractures outside the section under the maximum stress. In addition, on 0/0° sample, 4-point bending strength tests were performed at 1000 and 1500 °C in Ar flux to limit oxidation effect, by using a screw-driven load frame (Instron mod. 1195, Instron, USA). Test bars with dimensions 25 × 2.5 × as-processed thickness were fractured using a semi-articulated alumina 4-point fixture with a lower span of 20 mm and an upper span of 10 mm and at a cross-head rate of 1 mm/min.

The Young's modulus (E) and shear modulus (G) were measured using the sonic resonance method, according to ENV 843-2 standard. The test-piece was suspended in loops of cotton threads, using one loop to drive the vibration and the other to detect it. The resonant frequencies were measured on rectangular section bars of 60 mm × 10 mm × as-processed thickness using an impedance analyser (HP 4194A, USA).

2.4 Oxidation tests

Oxidation tests were carried out in a bottom loading furnace (FC18-0311281, Nannetti S.r.l., Italy) at 1650 °C in air for 1 min. 10 × 10 × as-processed thickness mm^3 plates were machined from 0/0°, 0/90° and 2D samples and cleaned with acetone in an ultrasonic bath. The specimens were placed on a porous zirconia sample holder, resting on one of the two largest surfaces, and introduced in the furnace when the target temperature was achieved and kept for 1 min. At the end of the oxidation test, the specimens were quickly removed and left to cool naturally in air. Specimens were weighed (accuracy ±0.01 mg) before and after oxidation test and the weigh difference was normalized over the initial surface area S, measured by calliper, by the equation: $\frac{\Delta m}{S} = \frac{w_{fin} - w_{in}}{S}$. The microstructures after oxidation were analysed similarly to non-oxidized samples by FE-SEM/EDS and XRD.

3. Results and discussion

2.1 Microstructural characterization

The final thickness of 0/0°, 0/90° and 2D plates was ~2.5 mm, 2.2 mm and 1.7 mm, respectively. Compositions, fibre volumetric amount (FVC), densities and residual porosities of the composites after 6 PIP cycles are reported in Table 1. The porosity of the impregnated preforms was initially around 40-50 vol.% and gradually decreased with the infiltration cycles. The final bulk densities were ~3.2 g/cm^3 for 0/0° and 0/90° and ~2.7 g/cm^3 for 2D, respectively. The porosity measured by mercury intrusion porosimetry was 6 vol.% for 0/0° and 0/90° and 9 vol.% for 2D. All the composites contained similar fractions of carbon fibres. UHTC (27-29%) and SiC (35-36%) phase contents were similar for 0/0° and 0/90° composites, whilst 2D samples contained a larger fraction of SiC, with consequent reduction of the bulk density. The higher content of SiC in the latter was certainly due to the lower extent of penetration of the UHTC slurry in the first step of impregnation.

X-Ray diffraction patterns (Fig. 2) collected on the surface of the three composites after the 6 PIP cycles were very similar (example in Fig. 2 refers to 2D samples) and confirmed the presence of ZrB_2 (PDF 65-3389) and graphite (PDF 26-1079), while the amorphous SiC(O) obtained by pyrolysis of polycarbosilane generated only a broad X-Ray scattering profile. No reflections from the α-SiC powder (introduced by slurry infiltration) were observed, due to the content below the minimum detectable. Detailed description of each composite typology is reported below.

Table 1. Composition, open porosity and Archimedes' density of the fabricated composites.

Sample label	**C_f (vol.%)**	**UHTC (vol.%)**	**SiC (vol.%)**	**Open porosity (%)**	**Bulk density (g/cm^3)**
0/0°	30±1	29±1	35±1	~6	3.2±0.2
0/90°	31±1	27±1	36±1	~6	3.2±0.2
2D	30±1	19±1	42±1	~9	2.7±0.3

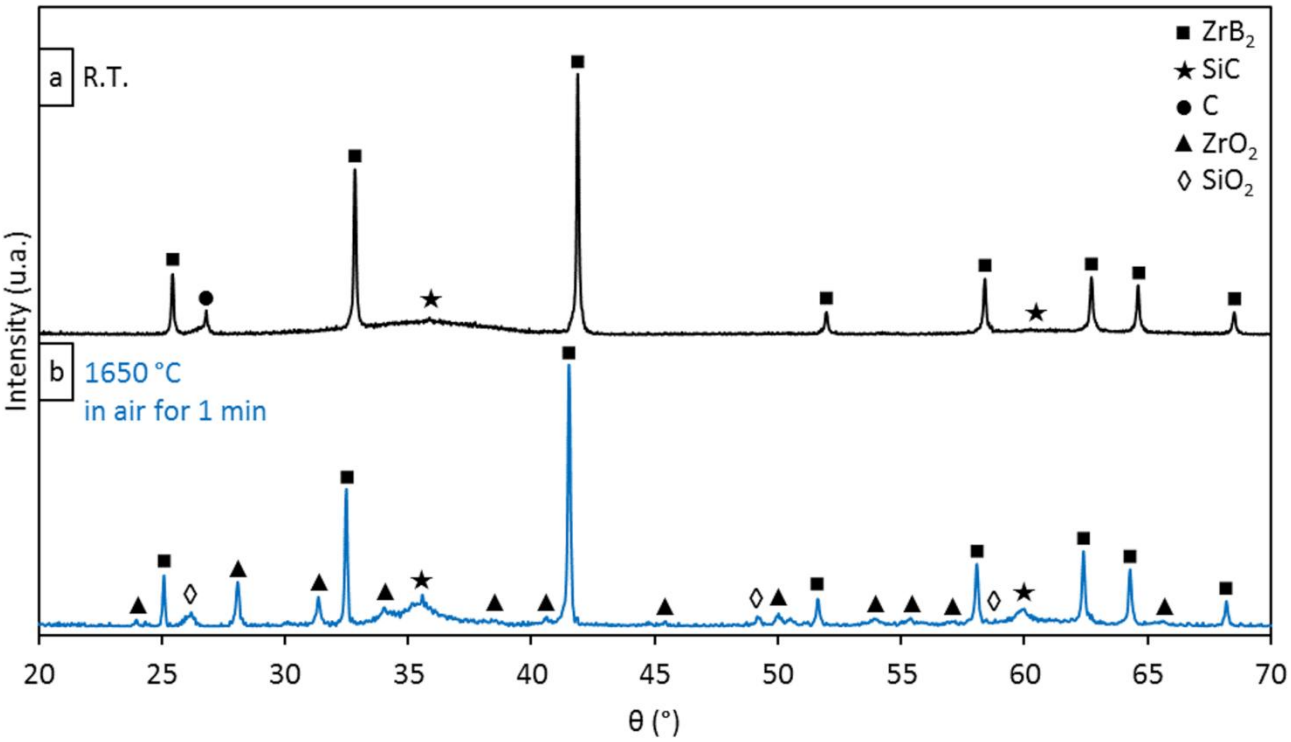

Fig. 2. X-ray diffraction patterns of the surface of 2D sample at R.T (a) and after oxidation tests at 1650 °C in air for 1 min (b).

0/0° composite: this sample achieved a bulk density of 3.2 g/cm^3 and a porosity around 6% (Fig. 3a-c). Polished cross sections (Fig. 3a) of the 90° side showed a homogeneous microstructure with regions infiltrated by the slurry alternated with polymer derived ceramic (PDC) and occasionally unfilled areas of 100-300 μm in size, probably due to air trapped during the stage of powder slurry infiltration. The 0° view (inset in Fig. 3a) revealed the presence of periodic cracks, formed during the drying stage after slurry infiltration. An enlarged view of the 90° section confirmed the homogenous distribution of carbon fibre, dark grey phase, in the matrix and evidenced the SiC(O) regions obtained by the precursor (Fig. 3b). The white contrasting phase is ZrB_2, the grey phases are SiC and SiC(O). SiC powder and SiC(O) are hardly distinguishable due to the low contrast between them. The good homogeneity of powder distribution in the material and the low level of defectiveness obtained with infiltration process are comparable (or even better) than other composites obtained with the PIP process [15,28,40]. A typical fibre/matrix interface is shown in Fig. 3c; the fibre was surrounded by a film of SiC(O) (a part is indicated as a yellow area in Fig. 3c), in which ZrB_2 particles are embedded. In any case the interface was quite smooth.

0/90° composite: this composite, illustrated in Fig. 3e,f,g, showed microstructural features similar to 0/0° sample in terms of density, homogenous dispersion of fibre in the matrix as well as powder mixture in SiC(O) matrix (see blue rectangle highlighting Fig. 3b,c,f,g). It can be noticed that the number of cracks increased due to additional stresses introduced by the 0/90° stacking configuration.

2D composite: this sample had a bulk density of 2.7 g/cm^3 and a porosity around 10%. The higher porosity was ascribed to the presence of voids in the waving structure of 2D fabrics. The resulting microstructure was less homogeneous than the previous cases, showing typical flaws of these composites (Fig. 3i): non-infiltrated intra-bundle regions and cracks in UHTC matrix-rich inter-bundles area. The powder slurry infiltration of 2D fabrics was less effective than in the case of UD fabrics, particularly in the central area of bundles. Accordingly, an inhomogeneous distribution of SiC(O) was achieved, with a higher content in the central part of bundles (see arrow Fig. 3i). Two different fibre/matrix interfaces were hence created for those composites: a ZrB_2-rich interface and a SiC(O)-rich interface, see Fig. 3g and Fig. 3m respectively. Both interfaces were relatively smooth, however SiC(O)-rich interface showed radial cracks and partial detachment of the SiC(O) phase from the C_f (see arrows in Fig. 3m). Two different contrasting SiC(O) phases, light grey and grey showed in Fig. 3m (see yellow lines), revealed a layered structure around the C_f, created by the repetitive infiltration and pyrolysis cycles. As already reported in previous works these defects were caused by shrinkage of preceramic polymers during pyrolysis (up to 50 vol.%) [32,41]. On the contrary, where SiC(O) was homogeneously mixed with ZrB_2 and SiC particles no cracks were found, see Fig. 3c,g. Detail of the UHTC-rich interface shows at least 200-300 nm film of SiC(O) between ZrB_2 particles and the fibre, see yellow lines in Fig. 3c. As expected, the size and shape of ZrB_2 and SiC particles, analysed by image analysis, were found similar to the starting raw powders due the relative mild conditions of pyrolysis (1000 °C). EDS analysis (Fig. 3n) on the SiC(O) confirm the presence of oxygen in the polymer-derived ceramic structure [42]. An oxygen content of approximately 15 at.% was estimated, in agreement with data given by SMP-10 supplier and as Kaur et al. revealed in [43]; moreover, further oxygen could derive from spurious oxides present on the surface of ZrB_2 and SiC particles. EDS analysis of ZrB_2 and SiC particles are reported in Fig. 3d,h. Image analysis showed a mean fibre diameter of consolidated composites perfectly in agreement with that of pristine fibre (Fig.3o). Hence the fibre was not strongly degraded by SiC(O) and its bimodal distribution, centred at 9.7 and 11.3 μm, can be seen in Fig. 3b,f,l.

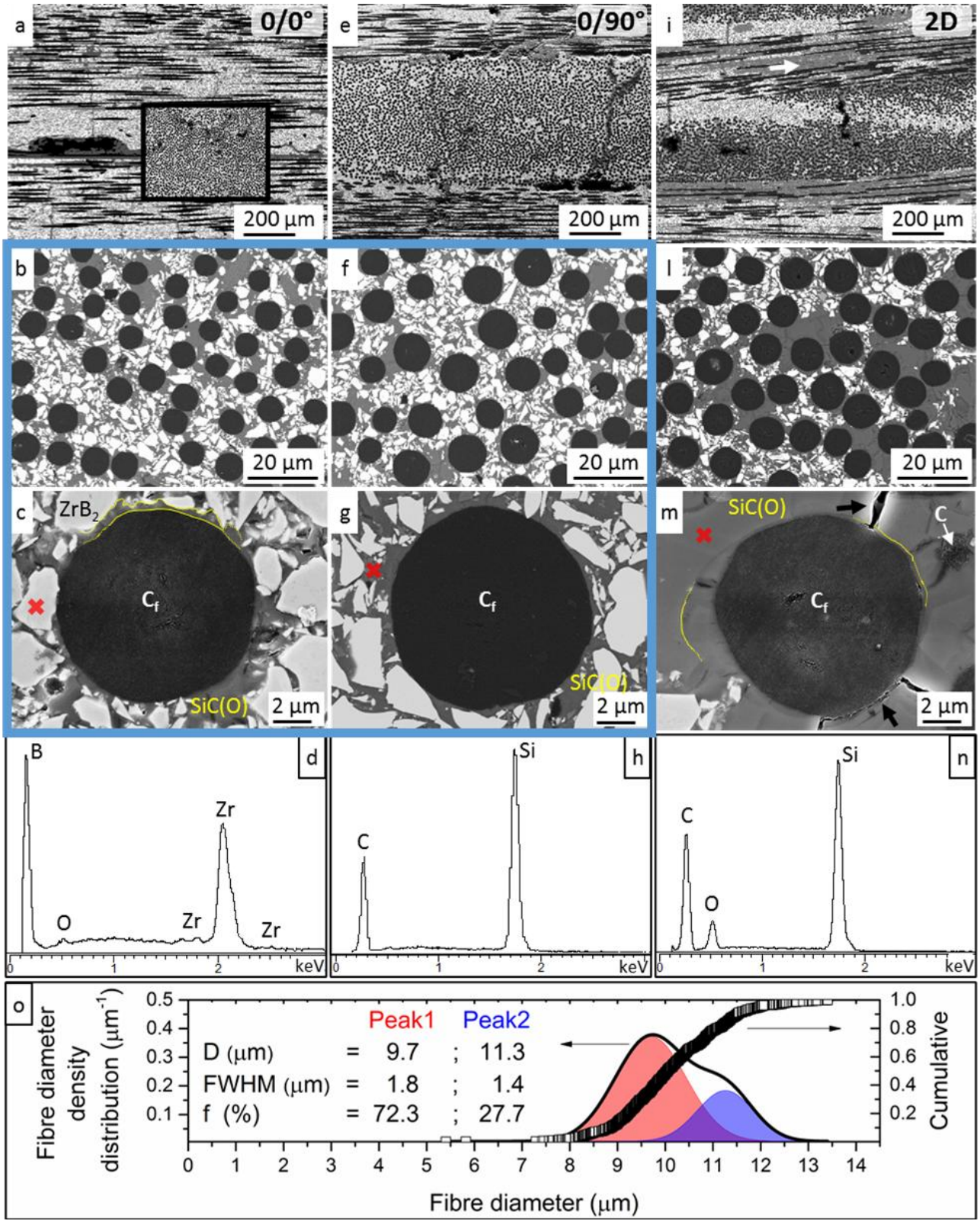

Fig. 3. Polished sections of C_f/ZrB_2-SiC composites obtained after 6 cycles of PIP. Low magnification micrographs of a) 0/0° sample, e) 0/90° sample and i) 2D sample; white arrow points a higher content of SiC(O) in intra-bundle regions. Details of microstructure of b) 0/0° sample, f) 0/90° sample, l) 2D sample. A single fibre surrounded by the matrix: c) ZrB_2-rich area in 0/0° sample, where a SiC(O) film around the C_f is shown (a part is indicated as a yellow area), g) ZrB_2-rich area in 0/90°, m) SiC(O)-rich area in 2D sample; yellow lines show the layered structure of SiC(O) due to repetitive PIP cycles, black arrows point cracks in SiC(O) and detachment between fibre and SiC(O) due to the shrinkage of preceramic polymer during

pyrolysis. d, h, n) EDS spectra (EDS spots were marked with red crosses in Fig. 3c,g,m), o) density distribution and cumulative curves of fibre diameter after PIP process.

Fig. 4a,b shows the typical fracture surfaces of 0/0° and 2D samples after 6 PIP cycles. The high homogeneity of the infiltration obtained for 0/0° is visible in the fracture surface shown in Fig.4a, the extent of fibre pull-out of tens of microns is reduced compared to the fracture of 2D sample reported in Fig. 4b. A more complex fracture is pointed out in Fig. 4b due to the presence of patchwork of SiC(O)-rich and powder-rich areas where fibre/matrix weak and strong interfaces are formed, respectively.

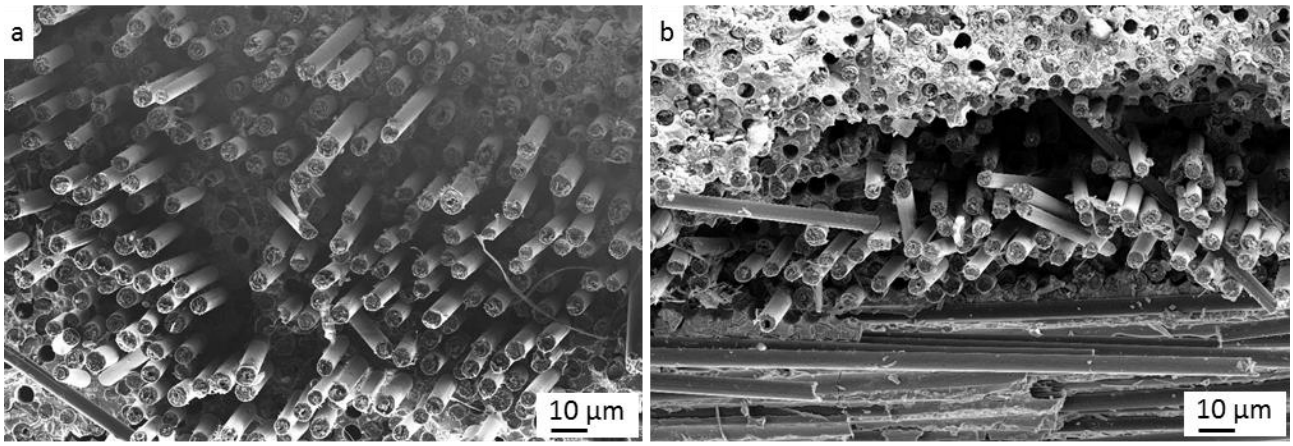

Fig. 4. Fracture surface micrographs of samples, a) 0/0°, and b) 2D, where an extensive and limited pull-out is shown at SiC(O)-rich and powder-rich interfaces respectively.

3.1 Mechanical properties

Stress-displacement curves of the bars tested at room temperature are reported in Fig. 5; mean values of maximum stress are reported in Table 2. As expected, the highest stress value was showed by 0/0° samples and it ranged from 429 to 523 MPa. The range of flexural strength values decreased down to 364-392 MPa in case of 0/90° composites. The lower flexural strength of 0/90° composites, as well as the lower slope of their curve, is expected due to the lower mechanical properties of C_f along the transverse direction. Both kinds of composites may have failed by a sequential combination of interlaminar shear and tensile modes. This was suggested by the sharp decrease of stress after its maximum value and the following gradual decrease or slightly increase [44]. The interlaminar shear contribution to the failure was more pronounced in case of 0/90° composites. The reasons can be ascribed to the higher number of cracks and the higher residual

stress between the stacked 0° and 90° layers that resulted in low-strength planes. On the other side, a 0/0° composite showed a graceful failure, suggesting that the span-to-thickness ratio of 20 is close to the minimum value to guarantee a valid flexural test. However, the curve characterized by a graceful failure showed two pop-ins at the early stage of the loading. Hence, the failure may have been influenced by a pop-in crack, which propagated from a critical flaw in the tensile surface and crossed the neutral axis without being deflected. According with the classical theory, the interlaminar shear stress achieved at the maximum load for 0/0° and 0/90° composites was 13.7 ±0.9 MPa and 9.1 ±0.5 MPa, respectively. For 2D composites, no sign of interlaminar shear failure was observed neither in the fractured specimens nor in the stress-displacement curves. Furthermore, all the fracture surfaces passed through the inter-bundle voids present on the tensile surface. The flexural strength values ranged from 170 to 221 MPa, and it is possible that were affected by these critical flaws, in addition to the lower amount of longitudinal fibre and their waviness. Also, the elastic moduli showed the tendency to decrease with decreasing the longitudinal fibre volumetric amount and increasing of the preforms complexity (Table 2).

The mechanical properties of these composites are similar or even better than those of similar CMCs produced by PIP (Table 2), though a direct comparison among flexural strengths is not fully reliable due to the different testing conditions, e.g. span/thickness ratio (s/t) and crosshead speed. For 0/90° configurations, a useful comparison is with a couple of materials studied in Ref. [28] by some of the authors of the present work. In detail, these composites were both pitch-based C fibre-reinforced ZrB_2-SiC. The first one was obtained by infiltration with a polymer-based SMP-10/ZrB_2 slurry and subsequent hot pressing, and with 55 vol.% of fibres, 27% of UHTC phase and 5% of porosity featured a bending strength of 152 MPa, e.g. half the resistance of the present work. The second one was obtained by infiltration of a water-based ZrB_2-SiC slurry and subsequent hot pressing, and with a 40 vol% fibres, 54 vol% of UHTC and 8% porosity exhibited a strength of 240 MPa, again lower than the present materials. The superior performance of the 0/90° samples of this work is certainly due to the better features of the matrix/fibre interface that allows a more efficient load transfer from the matrix to the fibres. In turn, this is related to the relatively mild conditions of pyrolysis, which allowed matrix consolidation and porosity reduction without fibre alteration. ~~although it was characterized by a microstructure similar to that of the present 0/90° sample, showed less than half resistance (Table 2). This lower flexural strength may be ascribed to the lower span/thickness ratio (s/t = 5)~~

~~that increased the interlaminar shear stress rate under loading with respect to the tensile stress rate in the outermost fibres~~ [28]. As for 2D architecture of similar materials, only 3-point bending tests were reported in literature [15,24,25,45]. Since inter-bundle voids are generally not under the load pin, the failure may occur beyond the cross section under the maximum bending moment, hence the flexural strength may be overestimated. However, the reported values go from 120 to 270 MPa. Hu et al. [15] developed C/SiC material enriched with about 25 vol.% ZrB_2 particles, and reported a flexural strength of 163 MPa. Wang et al. [24] obtained a strength of 237 ±30 MPa for 2D C_f/ZrB_2-SiC. L. Li et al. [25] reported a value of 255 ±15 MPa for 2D woven C_f/SiC enriched with a ZrB_2-TaC mixture. Q. Li et al. [45] developed a C_f/ZrC-SiC characterized by 34 vol.% of UTHC and 34 vol.% of carbon fibres and reported 143 ±21 MPa of flexural strength.

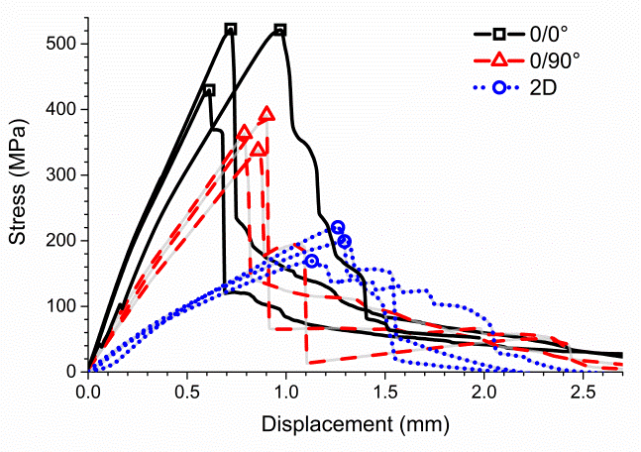

Fig. 5 Stress/displacement curves of 0/0° and 0/90° samples tested by 3-point bending, and 2D samples tested by 4-point bending. The point at the maximum stress was highlighted with a symbol.

Table 2. Microstructural and mechanical properties of C_f/ZrB_2-SiC composites.

Ref.	PIP cycles	Heat treatment	Carbon Fibre		Carbon preform architecture	UHTC powder	Porosity	Density	Bending strength, σ_f	Young's modulus, E	Shear modulus, G
	n°	°C	type	vol. %		vol.%	vol.%	g/cm^3	MPa	GPa	GPa
This work	6	1000	pitch	30	0/0°	29	6	3.2	491 ± 44	220 ± 9	25 ± 1
This work	6	1000	pitch	31	0/90°	27	6	3.2	364 ± 27	101 ± 19	17 ± 4
This work	6	1000	pitch	30	2D	19	9	2.7	188 ± 19	78 ± 13	11 ± 1
[28]	1	1900	pitch	55	0/90°	27	5	3.3	152 ± 12	-	-
[28]	0	1900	pitch	40	0/90°	54	8	3.9	235 ± 40	-	-
[15]	n.a.	1200	PAN	18.9	2D	25	23	2.6	163	24	-

4-point flexural strength at 1000 °C of 0/0° samples reached 600 ± 10 MPa. The higher value was related to the release of thermal residual stresses that can be developed during the cooling step of the

pyrolysis process owing to the coefficient of thermal expansion mismatch between carbon fibre and ceramic matrix [46]. At 1500 °C, 0/0° composites plastically deformed during 4-point bending test due to softening of glassy phases (e.g. B_2O_3, SiO_2 and borosilicate) present at grain boundaries of ZrB_2. 1500 °C is a temperature higher than T_g (glass transition temperature) of borosilicate glass, ~820 °C [47] and even of pure silica, ~1200 °C[48].

Since the PIP cycles were conducted at temperature as low as 1000°C it is expected that the matrix material is not completed converted to pure SiC. In the future, therefore, higher temperature PIP cycles will be studied in order to obtain the best compromise between stability of the material at high temperature and the lowest possible processing temperature.

3.2 Oxidation behaviour

Weight and dimensional variations of the specimens are reported in Table 1, while the micrographs of surfaces and cross sections are shown in Fig. 6, 7. After oxidation, all the samples exhibited similar weight loss, probably due to fibre volatilization and release of gaseous products. Common to all samples was also a slight volume increase.

Table 3. Mass variation, normalized to the initial surface area, and volume variation after oxidation test at 1650 °C in air.

	$\Delta m/S$ (mg/cm^2)	ΔV (cm^3)
0/0°	-11.6	+0.02
0/90°	-10.7	+0.01
2D	-6.9	+0.02

According to X-ray diffraction analysis, bulk ZrB_2 reflections were still visible for all the specimens due to the low extent of oxidation, see the spectrum in Fig. 2b. Moreover, monoclinic ZrO_2 peaks were also detected (PDF 65–1025). The evolution of amorphous SiC(O) was more difficult to track because the air exposed part was converted mainly into borosilicate glass while the underlying part was found crystallized into β-SiC (PDF 65-0360) and SiO_2 (PDF 12-0708) [49]. No carbon reflections were detected after exposure at 1650 °C. According to SEM analysis, oxidised surfaces displayed similar features amongst the samples (Fig. 6a,b): fibres close to the surface or onto the surface were volatilized leaving voids. The surface was almost entirely covered with a borosilicate (BS) glassy phase, which embedded scattered residues of SiC(O)

phase from the polycarbosilane, found on the specimen surface after pyrolysis. The borosilicate glass flowed in the grooves and filled the voids. Glass diffusion form the subsurface towards the surface and consequent bubble formation/explosion left tiny ZrO_2 grains embedded in the glass, as common for oxidised ZrB_2-SiC materials [50] (Fig. 6c).

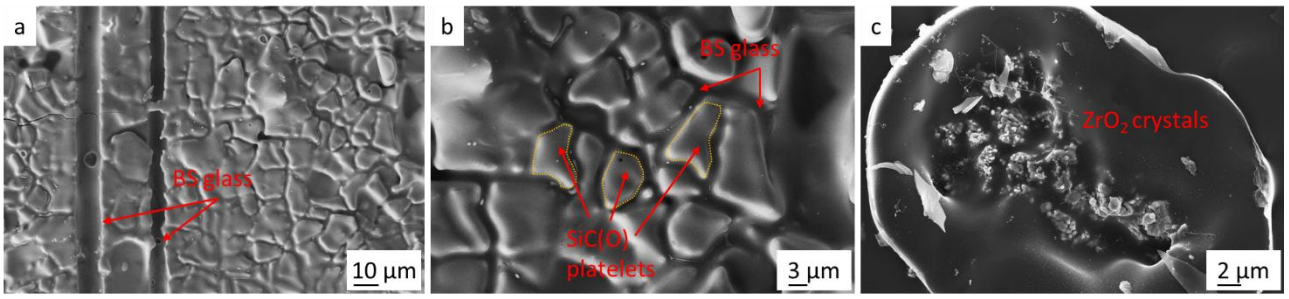

Fig. 6. Features of the sample surface oxidized at 1650 °C showing self-healing effects. a) Fibre evaporation and voids partially filled by the BS glassy phase (BS=borosilicate), b) magnified view showing the BS glass flowing in the grooves left by the SiC(O) phase, c) bubble with tiny zirconia crystals.

Cross sections (Fig. 7a-d) of the oxidised samples were similar to other C_f/ZrB_2-SiC composites exposed to air furnace at 1650 °C [51], e.g. they were featured by a layered structure comprising an external borosilicate glass layer with variable thickness, an intermediate zirconia-silica scale, where the holes left by the fibre oxidation were partially filled by the glass, and the unreacted matrix scale (Fig. 7b). The thickness of the oxidized layer was not constant in these samples because it was affected by the bulk homogeneity. For instance, for 0/0° and 0/90° samples it was around 50 µm, whilst for 2D samples, the modified layer thickness was very irregular spanning from 10 to 100 µm (Fig. 7c,d), depending on the local constituent phases. Moreover, cross section details revealed that fibres close to the exposed surface were volatilized leaving voids for 0/0° samples which were then partially filled with the borosilicate glass (Fig. 7b). On the contrary, in regions where the fibres were covered with the ZrB_2 and SiC(O), fibres were fully protected from oxidation (see Fig. 7d). Again, the function of the borosilicate glass was evident in closing big cracks (Fig. 7c) and in encasing the scattered platelets of SiC(O) phase on the surface.

As said, samples were introduced when the furnace reached the final temperature, e.g. 1650 °C. With the furnace opening, the temperature slightly decreased, to ~1500 °C but in a bunch of seconds it recovered the final temperature. In these conditions, all competing oxidation phenomena occurred almost instantly. In detail, they were: vaporization of carbon fibre in the surface (Reaction 1), oxidation of ZrB_2 to crystalline

zirconia and boron oxide (Reaction 2), oxidation of SiC to silica (Reaction 3), formation of a borosilicate glass (Reaction 4).

$$C(s) + 1/2(g) \rightarrow 2CO(g) \quad (1)$$

$$ZrB_2(s) + 5/2O_2(g) \rightarrow ZrO_2(s) + B_2O_3(l,g) \quad (2)$$

$$SiC(s) + 3/2O_2(g) \rightarrow SiO_2(s) + CO(g) \quad (3)$$

$$SiO_2(s) + B_2O_3(l) \rightarrow SiO_2\text{-}B_2O_3(l), \quad (4)$$

The observed weight variations were thus the results of weight increase due to formation of zirconia, silica and boria, and weight decrease due to fibre vaporization and other CO(g) formation from Reaction 3. Noteworthy, the formation of the borosilicate glass allowed crack closure, closure of pores left by the fibre, demonstrating the self-healing ability of these composites.

Comparing these oxidation results to previous UHTCMCs samples with 0/90° structure, but different composition (46 vol.% ZrB_2, 12 vol.% SiC, 37 vol.% C_f, 5 vol.% pores) oxidized at 1650 °C in air in the same furnace [51], we found similar or even lower thickness of the oxidised layer for the materials of the present work. In contrast, weight loss was more marked (-10 mg/cm^2 this work vs -2.4 mg/cm^2 in [51]). We speculate that additional weight loss could be due to the volatilization of gaseous species during crystallization of the bulk underlying SiC(O) occurring all through the sample bulk at 1650 °C. The relatively mild pyrolysis conditions (1000 °C) very likely did not allow full conversion of the polymer into ceramic, which may be partially hydrogenated (e.g. Si-CH_3 and Si-OH groups), when pyrolyzed at insufficiently high temperature [49]. This was also confirmed by the elevated temperature mechanical properties results.

In a previous work [28], we tried to define the most important factors that may enhance the matrix efficacy in protecting the most vulnerable phase, e.g. C fibres. These factors were:

I) C fibres must be circumvented by the protective ZrB_2-SiC matrix;

II) the matrix should have a low open porosity (<10%) to hinder oxygen penetration;

III) fibre content does not exceed the matrix content.

The results obtained here indicate that these criteria (found for sintered UHTCMCs) hold true also for samples processed by PIP, the only difference being the different SiC/ZrB_2 phase volumetric ratio. Although 1650 °C is a still a relatively mild temperature for the UHTC refractoriness, the addition of ZrB_2 was

essential for the formation of the ZrO_2-enriched borosilicate layer that played the important function of closing pores and cracks, in the surface and subsurface layer.

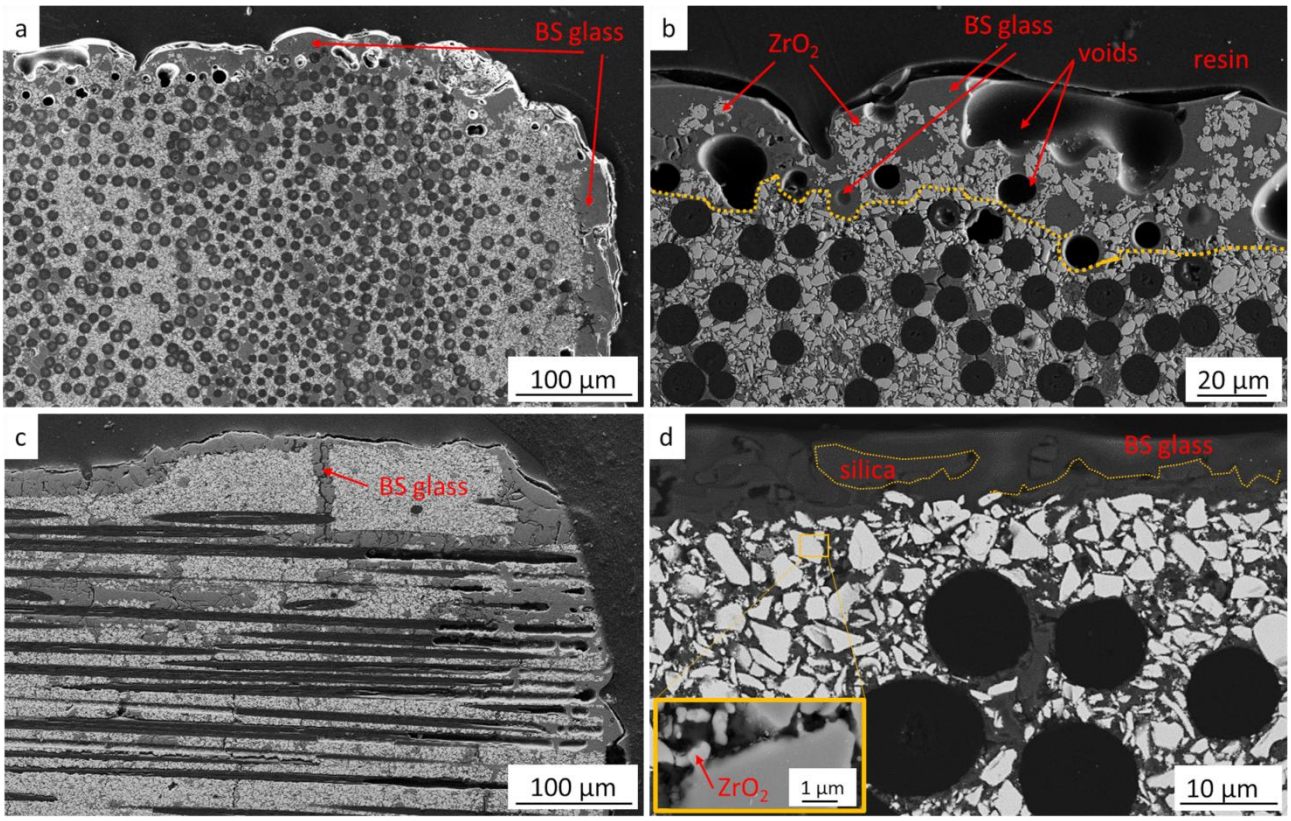

Fig. 7. Cross sections of 0/0° and 2D samples after oxidation at 1650 °C/1 min: a) overview of 0/0° sample showing the sample coverage by the glassy phase, b) enlarged view showing the ZrO_2-borosilicate layer and voids left by the fibres partially replace by glassy phase. c) overview of 2D sample, d) detail showing bi-composition of the scale constituted of the silica plates encased in borosilicate phase (darker) and fully protected fibres underneath the scale. Inset shows partially oxidised ZrB_2 particles.

4. Conclusions

In this work, pitch-based carbon fibres reinforced 20-30 vol.% ZrB_2-enriched composites were fabricated via slurry infiltration (water based) coupled with polymer infiltration and pyrolysis at relatively low temperatures. Composites obtained using unidirectional fabrics (0/0° and 0/90°) had a bulk density of 3.2 g/cm^3 and a residual open porosity of ~6%. Good homogeneity of ZrB_2 distribution and low defectiveness were achieved. As expected, the composite obtained using plain woven fabrics made with very stiff fibres led to a less homogeneous microstructure, higher porosity (~10%) and consequently lower bulk density of 2.7 g/cm^3.

The mechanical properties, including bending strength, elastic and shear modulus, were critically evaluated. The performance showed the tendency to decrease with increase of the C_f preform complexity. For instance, the flexural strength was approaching 500 MPa for 0/0°, 370 MPa for 0/90° and 190 MPa for 2D.

Moreover, preliminary mechanical tests at elevated temperature indicated that oxides impurities have a strong impact on material performance at extremely hot environments, consequently further optimizations are necessary. Nevertheless, self-healing functionality, typical of sintered ZrB_2-SiC systems, was achieved also for these materials obtained at mild conditions. After exposing the material at 1650 °C in air for 1 min the matrix surface was covered by a low viscous borosilicate glass scale which closed pores, cracks and prevented fibres burn out, showing an optimal resistance to oxidation.

Declaration of Competing Interests

The authors declare that they have no known competing financial interests or personal relationships that could have appeared to influence the work reported in this paper.

Acknowledgements

Authors wish to thank A. Piancastelli, M. Mazzocchi and C. Melandri for technical support. This work is partially funded by the European Union's Horizon 2020 "Research and innovation programme" under grant agreement No 685594 (C3HARME: Next Generation Ceramic Composites for Harsh Combustion Environment and Space).

References

[1] W.G. Fahrenholtz, E.J. Wuchina, W.E. Lee, Y. Zhou, Ultra-High Temperature Ceramics: Materials for Extreme Environment Applications, John Wiley & Sons, Inc., Hoboken, New Jersey, 2014. doi:10.1002/9781118700853.

[2] M.M. Opeka, I.G. Talmy, E.J. Wuchina, J.A. Zaykoski, S.J. Causey, Mechanical, Thermal, and

Oxidation Properties of Refractory Hafnium and zirconium Compounds, J. Eur. Ceram. Soc. 19 (1999) 2405–2414. doi:10.1016/S0955-2219(99)00129-6.

[3] W.G. Fahrenholtz, G.E. Hilmas, I.G. Talmy, J.A. Zaykoski, Refractory diborides of zirconium and hafnium, J. Am. Ceram. Soc. 90 (2007) 1347–1364. doi:10.1111/j.1551-2916.2007.01583.x.

[4] S.R. Levine, E.J. Opila, M.C. Halbig, J.D. Kiser, M. Singh, J.A. Salem, Evaluation of ultra-high temperature ceramics for aeropropulsion use, J. Eur. Ceram. Soc. 22 (2002) 2757–2767. doi:10.1016/S0955-2219(02)00140-1.

[5] B.R. Golla, A. Mukhopadhyay, B. Basu, S.K. Thimmappa, Review on ultra-high temperature boride ceramics, Prog. Mater. Sci. 111 (2020) 100651. doi:10.1016/j.pmatsci.2020.100651.

[6] A.L. Chamberlain, W.G. Fahrenholtz, G.E. Hilmas, D.T. Ellerby, Characterization of zirconium diboride for thermal protection systems, Key Eng. Mater. 264–268 (2004) 493–496. doi:10.4028/www.scientific.net/kem.264-268.493.

[7] W.G. Fahrenholtz, G.E. Hilmas, Oxidation of ultra-high temperature transition metal diboride ceramics, Int. Mater. Rev. 57 (2012) 61–72. doi:10.1179/1743280411Y.0000000012.

[8] P. Hu, W. Guolin, Z. Wang, Oxidation mechanism and resistance of ZrB_2-SiC composites, Corros. Sci. 51 (2009) 2724–2732. doi:10.1016/j.corsci.2009.07.005.

[9] W. Krenkel, Ceramic Matrix Composites, Wiley-VCH, Weinheim, 2008. doi:10.1002/9783527622412.

[10] S. Kumar, K.C. Shekar, B. Jana, L.M. Manocha, N. Eswara Prasad, C/C and C/SiC Composites for Aerospace Applications, in: R.J.H.W. N. Eswara Prasad (Ed.), Aerosp. Mater. Mater. Technol. Vol. 1 Aerosp. Mater., Springer, Singapore, 2017: pp. 343–369. doi:10.1007/978-981-10-2134-3_15.

[11] Y. Arai, R. Inoue, K. Goto, Y. Kogo, Carbon fiber reinforced ultra-high temperature ceramic matrix composites: A review, Ceram. Int. 45 (2019) 14481–14489.

[12] S. Tang, J. Deng, S. Wang, W. Liu, K. Yang, Ablation behaviors of ultra-high temperature ceramic composites, Mater. Sci. Eng. A. 465 (2007) 1–7. doi:10.1016/j.msea.2007.02.040.

[13] A. Paul, S. Venugopal, J.G.P. Binner, B. Vaidhyanathan, A.C.J. Heaton, P.M. Brown, UHTC-carbon fibre composites: Preparation, oxyacetylene torch testing and characterisation, J. Eur. Ceram. Soc. 33 (2013) 423–432. doi:10.1016/j.jeurceramsoc.2012.08.018.

[14] V. Rubio, J. Binner, S. Cousinet, G. Le Page, T. Ackerman, A. Hussain, P. Brown, I. Dautremon, Materials characterisation and mechanical properties of Cf-UHTC powder composites, J. Eur. Ceram. Soc. 39 (2019) 813–824.

[15] H. Hu, Q. Wang, Z. Chen, C. Zhang, Y. Zhang, J. Wang, Preparation and characterization of C/SiC-ZrB2 composites by precursor infiltration and pyrolysis process, Ceram. Int. 36 (2010) 1011–1016. doi:10.1016/j.ceramint.2009.11.015.

[16] Q. Li, S. Dong, Z. Wang, G. Shi, Fabrication and properties of 3-D Cf/ZrB_2-ZrC-SiC composites via polymer infiltration and pyrolysis, Ceram. Int. 39 (2013) 5937–5941. doi:10.1016/j.ceramint.2012.11.074.

[17] F. Uhlmann, C. Wilhelmi, S. Schmidt-Wimmer, S. Beyer, C. Badini, E. Padovano, Preparation and characterization of ZrB_2 and TaC containing Cf/SiC composites via Polymer-Infiltration-Pyrolysis process, J. Eur. Ceram. Soc. 37 (2017) 1955–1960. doi:10.1016/j.jeurceramsoc.2016.12.048.

[18] N. Patra, N. Al Nasiri, D.D. Jayaseelan, W.E. Lee, Thermal properties of Cf/HfC and Cf/HfC-SiC composites prepared by precursor infiltration and pyrolysis, J. Eur. Ceram. Soc. 38 (2018) 2297–2303. doi:10.1016/j.jeurceramsoc.2017.12.051.

[19] M. Kütemeyer, L. Schomer, T. Helmreich, S. Rosiwal, D. Koch, Fabrication of ultra high temperature ceramic matrix composites using a reactive melt infiltration process, J. Eur. Ceram. Soc. 36 (2016) 3647–3655. doi:10.1016/j.jeurceramsoc.2016.04.039.

[20] X. Chen, S. Dong, Y. Kan, X. Jin, H. Zhou, D. Ni, D. Wang, Microstructure and mechanical properties of three dimensional Cf/SiC-ZrC-ZrB_2 composites prepared by reactive melt infiltration method, J. Eur. Ceram. Soc. 36 (2016) 3969–3976. doi:10.1016/j.jeurceramsoc.2016.07.002.

[21] S. Zhang, S. Wang, W. Li, Y. Zhu, Z. Chen, Preparation of ZrB_2 based composites by reactive melt infiltration at relative low temperature, Mater. Lett. (2011). doi:10.1016/j.matlet.2011.06.070.

[22] L. Zoli, A. Vinci, P. Galizia, C. Melandri, D. Sciti, On the thermal shock resistance and mechanical properties of novel unidirectional UHTCMCs for extreme environments, Sci. Rep. submitted (2018).

[23] P. Hu, D. Zhang, S. Dong, Q. Qu, X. Zhang, A novel vibration-assisted slurry impregnation to fabricate Cf/ZrB2-SiC composite with enhanced mechanical properties, J. Eur. Ceram. Soc. 39 (2019) 798–805. doi:10.1016/j.jeurceramsoc.2018.10.029.

[24] Y. Wang, W. Liu, L. Cheng, L. Zhang, Preparation and properties of 2D C/ZrB_2-SiC ultra high temperature ceramic composites, Mater. Sci. Eng. A. 524 (2009) 129–133. doi:10.1016/j.msea.2009.07.005.

[25] L. Li, Y. Wang, L. Cheng, L. Zhang, Preparation and properties of 2D C/SiC-ZrB_2-TaC composites, Ceram. Int. 37 (2011) 891–896. doi:10.1016/j.ceramint.2010.10.033.

[26] L.M. Rueschhoff, C.M. Carney, Z.D. Apostolov, M.K. Cinibulk, Processing of fiber-reinforced ultra-high temperature ceramic composites: A review, Int. J. Ceram. Eng. Sci. (2020). doi:10.1002/ces2.10033.

[27] D. Zhang, P. Hu, S. Dong, X. Liu, C. Wang, Z. Zhang, X. Zhang, Oxidation behavior and ablation mechanism of Cf/ZrB2-SiC composite fabricated by vibration-assisted slurry impregnation combined with low-temperature hot pressing, Corros. Sci. 161 (2019) 108181. doi:10.1016/j.corsci.2019.108181.

[28] L. Zoli, D. Sciti, Efficacy of a ZrB_2–SiC matrix in protecting C fibres from oxidation in novel UHTCMC materials, Mater. Des. 113 (2017) 207–213. doi:10.1016/j.matdes.2016.09.104.

[29] L. Zoli, A. Vinci, L. Silvestroni, D. Sciti, M. Reece, S. Grasso, Rapid spark plasma sintering to produce dense UHTCs reinforced with undamaged carbon fibres, Mater. Des. 130 (2017) 1–7. doi:10.1016/j.matdes.2017.05.029.

[30] L. Ping Ran, F. Rao, K. Peng, H. Yin, M. Zhong Yi, Preparation and properties of C/C−ZrB_2−SiC composites by high-solid-loading slurry impregnation and polymer infiltration and pyrolysis (PIP), Trans. Nonferrous Met. Soc. China (English Ed. 29 (2019) 2141–2150. doi:10.1016/S1003-6326(19)65120-4.

[31] T. Reimer, I. Petkov, D. Koch, M. Fließ, C. Dellin, Fabrication and characterization of C/C-SiC material made with pitch-based carbon fibers, Ceram. Trans. 252 (2015) 277–293. doi:10.1002/9781119183860.ch28.

[32] B. Mainzer, C. Lin, R. Jemmali, M. Frieß, R. Riedel, D. Koch, Characterization and application of a novel low viscosity polysilazane for the manufacture of C- and SiC-fiber reinforced SiCN ceramic matrix composites by PIP process, J. Eur. Ceram. Soc. 39 (2019) 212–221. doi:10.1016/j.jeurceramsoc.2018.09.042.

[33] Y. Huang, R.J. Young, Effect of fibre microstructure upon the modulus of PAN- and pitch-based carbon fibres, Carbon N. Y. (1995). doi:10.1016/0008-6223(94)00109-D.

[34] D.D.L. Chung, 8 - Ceramic-Matrix Composites, in: D.D.L. Chung (Ed.), Carbon Compos., 2nd Ed., Butterworth-Heinemann, 2017: pp. 467–531. doi:https://doi.org/10.1016/B978-0-12-804459-9.00008-7.

[35] D. Zhang, P. Hu, S. Dong, Q. Qu, X. Zhang, Effect of pyrolytic carbon coating on the microstructure and fracture behavior of the Cf/ZrB_2-SiC composite, Ceram. Int. 44 (2018) 19612–19618. doi:10.1016/J.CERAMINT.2018.07.210.

[36] C. Fellah, J. Braun, C. Sauder, F. Sirotti, M.-H. Berger, Influence of the carbon interface on the mechanical behavior of SiC/SiC composites, Compos. Part A Appl. Sci. Manuf. 133 (2020) 105867. doi:10.1016/j.compositesa.2020.105867.

[37] Y. Zhou, W.C. Zhou, F. Luo, D.M. Zhu, Effects of dip-coated BN interphase on mechanical properties of SiC f/SiC composites prepared by CVI process, Trans. Nonferrous Met. Soc. China (English Ed. 24 (2014) 1400–1406. doi:10.1016/S1003-6326(14)63205-2.

[38] D. Sciti, L. Pienti, A. Natali Murri, E. Landi, V. Medri, L. Zoli, From random chopped to oriented continuous SiC fibers-ZrB_2 composites, Mater. Des. 63 (2014). doi:10.1016/j.matdes.2014.06.037.

[39] G. Stantschev, M. Frieß, R. Kochendörfer, W. Krenkel, Long fibre reinforced ceramics with active fillers and a modified intra-matrix bond based on the LPI process, J. Eur. Ceram. Soc. 25 (2005) 205–209. doi:10.1016/j.jeurceramsoc.2004.08.014.

[40] J.-F. Justin, A. Julian-Jankowiak, V. Guérineau, V. Mathivet, A. Debarre, Ultra-high temperature ceramics developments for hypersonic applications, CEAS Aeronaut. J. (2020). doi:10.1007/s13272-020-00445-y.

[41] L. Zoli, D. Sciti, L.A. Liew, K. Terauds, S. Azarnoush, R. Raj, Additive Manufacturing of Ceramics Enabled by Flash Pyrolysis of Polymer Precursors with Nanoscale Layers, J. Am. Ceram. Soc. 99 (2016) 57–63. doi:10.1111/jace.13946.

[42] P. Colombo, G. Mera, R. Riedel, G.D. Sorarù, Polymer-derived ceramics: 40 Years of research and innovation in advanced ceramics, J. Am. Ceram. Soc. 93 (2010) 1805–1837. doi:10.1111/j.1551-2916.2010.03876.x.

[43] S. Kaur, R. Riedel, E. Ionescu, Pressureless fabrication of dense monolithic SiC ceramics from a polycarbosilane, J. Eur. Ceram. Soc. 34 (2014) 3571–3578. doi:10.1016/j.jeurceramsoc.2014.05.002.

[44] Y. Lin, C. Liu, H. Li, K. Jin, J. Tao, Interlaminar failure behavior of GLARE laminates under double beam five-point-bending load, Compos. Struct. 201 (2018) 79–85. doi:10.1016/j.compstruct.2018.06.037.

[45] Q. Li, S. Dong, P. He, H. Zhou, Z. Wang, J. Yang, B. Wu, J. Hu, Mechanical properties and microstructures of 2D Cf/ZrC-SiC composites using ZrC precursor and polycarbosilane, Ceram. Int. 38 (2012) 6041–6045. doi:10.1016/j.ceramint.2012.04.005.

[46] P. Galizia, L. Zoli, D. Sciti, Impact of residual stress on thermal damage accumulation, and Young's modulus of fiber-reinforced ultra-high temperature ceramics, Mater. Des. 160 (2018) 803–809. doi:10.1016/J.MATDES.2018.10.019.

[47] V.O. Altemose, 7. Glass Vacuum Systems, in: G.L. Weissler, R.W. Carlson (Eds.), Vac. Phys. Technol., Academic Press, 1980: pp. 313–343. doi:10.1016/S0076-695X(08)60376-2.

[48] M.I. Ojovan, Glass formation in amorphous SiO_2 as a percolation phase transition in a system of network defects, JETP Lett. 79 (2004) 632–634. doi:10.1134/1.1790021.

[49] G. Chollon, Oxidation behaviour of polymer-derived ceramics, in: P. Colombo and R. Riedel and G. D. Soraru and H.-J. Kleebe (Ed.), Polym. Deriv. Ceram. From Nano-Structure to Appl., DEStech Publications, 2010: pp. 292–308.

[50] E. Opila, S. Levine, J. Lorincz, Oxidation of ZrB_2- And HfB_2-based ultra-high temperature ceramics: Effect of Ta additions, J. Mater. Sci. 39 (2004) 5969–5977. doi:10.1023/B:JMSC.0000041693.32531.d1.

[51] A. Vinci, L. Zoli, D. Sciti, Influence of SiC content on the oxidation of carbon fibre reinforced ZrB_2/SiC composites at 1500 and 1650 °C in air, J. Eur. Ceram. Soc. 38 (2018) 3767–3776. doi:10.1016/j.jeurceramsoc.2018.04.064.